

## Tetrahedrally coordinated boron in tourmalines from the liddicoatite-elbaite series from Madagascar: Structure, chemistry, and infrared spectroscopic studies

ANDREAS ERTL,<sup>1,\*</sup> JOHN M. HUGHES,<sup>2</sup> STEFAN PROWATKE,<sup>3</sup> THOMAS LUDWIG,<sup>3</sup>  
PINNELLI S.R. PRASAD,<sup>4</sup> FRANZ BRANDSTÄTTER,<sup>5</sup> WILFRIED KÖRNER,<sup>6</sup> RALF SCHUSTER,<sup>7</sup>  
FRANZ PERTLIK,<sup>1</sup> AND HORST MARSCHALL<sup>3</sup>

<sup>1</sup>Institut für Mineralogie und Kristallographie, Geozentrum, Universität Wien, Althanstrasse 14, 1090 Vienna, Austria

<sup>2</sup>Department of Geology, Miami University, Oxford, Ohio 45056, U.S.A.

<sup>3</sup>Mineralogisches Institut, Universität Heidelberg, Im Neuenheimer Feld 236, 69120 Heidelberg, Germany

<sup>4</sup>Gas Hydrates Division, National Geophysical Research Institute, Hyderabad 500 007, India

<sup>5</sup>Mineralogisch-Petrographische Abteilung, Naturhistorisches Museum, Burggring 7, 1014 Vienna, Austria

<sup>6</sup>Institut für Geochemie, Geozentrum, Universität Wien, Althanstrasse 14, 1090 Vienna, Austria

<sup>7</sup>Geologische Bundesanstalt, Rasumovskigasse 23, 1030 Vienna, Austria

### ABSTRACT

Four colorless tourmalines of the liddicoatite-elbaite series from pegmatites from Anjanabonoina, Madagascar, have been characterized by crystal-structure determination and by chemical analyses. Optimized formulae range from  $^X(\text{Ca}_{0.57}\text{Na}_{0.29}\square_{0.14})^Y(\text{Al}_{1.41}\text{Li}_{1.33}\text{Mn}_{0.07}^2\square_{0.19})^Z\text{Al}_6^T(\text{Si}_{5.86}\text{B}_{0.14})\text{O}_{18}(\text{BO}_3)_3^V(\text{OH})_{3.00}^W[\text{F}_{0.76}(\text{OH})_{0.24}]$  [ $a = 15.8322(3)$ ,  $c = 7.1034(3)$  Å] to  $^X(\text{Na}_{0.46}\text{Ca}_{0.30}\square_{0.24})^Y(\text{Al}_{1.82}\text{Li}_{0.89}\text{Fe}_{0.01}^2\text{Mn}_{0.01}^2\square_{0.27})^Z\text{Al}_6^T(\text{Si}_{5.56}\text{B}_{0.44})\text{O}_{18}(\text{BO}_3)_3^V(\text{OH})_{3.00}^W[(\text{OH})_{0.50}\text{F}_{0.50}]$  [ $a = 15.8095(9)$ ,  $c = 7.0941(8)$  Å] ( $R = 1.3$ – $1.7\%$ ). There is a high negative correlation ( $r^2 = 0.984$ ) between the  $\langle\text{T-O}\rangle$  bond-lengths ( $\sim 1.618$ – $1.614$  Å) and the amount of  $^IV\text{B}$  (from the optimized formulae). Similar to the olenites (from Koralpe, Austria) the liddicoatite-elbaite samples show a positive correlation between the Al occupancy at the Y site and  $^IV\text{B}$  ( $r^2 = 0.988$ ). Short-range order configurations show that the presence of  $^IV\text{B}$  is coupled with the occupancy of  $(\text{Al}_2\text{Li})$  and  $(\text{Al}_2\square)$  at the Y site. The structural formulae of the Al-rich tourmalines from Anjanabonoina, Madagascar, show  $\sim \square_{0.2}$  (vacancies) on the Y site. We believe that short-range order configurations with  $^Y(\text{Al}_2\square)$  are responsible for these vacancies. Hence, an oft-used calculation of the Li content by difference on the Y site may be problematic for Al-rich tourmalines (olenite, elbaite, rossmanite). Fourier transform infrared (FTIR) spectra were recorded from the most  $^IV\text{B}$ -rich tourmaline sample. The bands around  $5195$  and  $5380$   $\text{cm}^{-1}$  can be assigned to  $\text{H}_2\text{O}$ . Because these bands still could be observed in FTIR spectra at temperatures from  $-150$  to  $+600$  °C, it seems unlikely that they result from  $\text{H}_2\text{O}$  in fluid inclusions. Interestingly, another FTIR spectrum from a dravite in which the X site is filled completely with Na, does not show bands at  $\sim 5200$  and  $\sim 5400$   $\text{cm}^{-1}$ . Although not definitive, the resulting spectra are consistent with small amounts of  $\text{H}_2\text{O}$  at the X site of the elbaite. The rare-earth element (REE) pattern of the B-rich elbaite ( $\Sigma\text{REE}$ :  $\sim 150$  ppm) demonstrates that this sample is strongly enriched in LREEs compared to HREEs and exhibits a negative Eu anomaly. This sample shows the strongest enrichment of LREEs and a high  $\text{La}_N/\text{Yb}_N$  ratio of  $\sim 351$ , which seems to confirm an important role of the fractional crystallization process.

**Keywords:** Liddicoatite-elbaite, tetrahedrally coordinated boron, Madagascar, structure, chemistry

### INTRODUCTION AND PREVIOUS WORK

Tetrahedrally coordinated B in tourmaline was only first fully documented in 1997 (Ertl et al. 1997). In 1996, when *Boron: Mineralogy, Petrology, and Geochemistry* (Reviews in Mineralogy, vol. 33) was published, studies had “not provided compelling evidence” for  $^IV\text{B}$  (Henry and Dutrow 1996, p. 504). Of great significance are the implications for understanding why some tourmalines incorporate  $^IV\text{B}$  and others do not. In this work, we provide detailed models with short-range orders to explain the relationship between the occupancy at the Y site and the T site.

These short-range orders imply also that an oft-used calculation of the Li content by difference on the Y site may be problematic for Al-rich tourmalines (olenite, elbaite, rossmanite) because these tourmalines can contain vacancies at this site. It can also be problematic to normalize such tourmalines to 6.00 Si apfu by ignoring B non-stoichiometry, especially when they contain only low amounts of Fe, Mn, and the Al content at the Y site exceeds 1.3 apfu.

Tourmalines that contain  $^IV\text{B}$  were described recently from several localities. From a pegmatite near Stoffhütte, Koralpe, Styria, Austria, olenite samples with up to  $\sim 1$  apfu  $^IV\text{B}$  were described (Ertl et al. 1997; Hughes et al. 2000, 2004; Kalt et al. 2001; Marler and Ertl 2002). Additionally, schorl with  $\sim 0.25$  apfu  $^IV\text{B}$  was described from the same locality (Ertl and Hughes

\* E-mail: andreas.ertl@a1.net

2002). Olenite from a pegmatite at Olenii Ridge, Russia, was shown to contain ~0.40 apfu <sup>IV</sup>B (Schreyer et al. 2002). Elbaite samples from the Brown Derby pegmatite, Colorado, and from Mount Mica, Maine (Tagg et al. 1999; Hughes et al. 2001) show similar amounts of <sup>IV</sup>B. "Oxy-rossmanite" from a pegmatite near Eibenstein an der Thaya, Lower Austria, like olenite a tourmaline with a very high Al content, contains ~0.25 apfu <sup>IV</sup>B (Ertl et al. 2005). Metamorphic dravite (associated with omphacite) from Syros, Greece, contains ~0.17 apfu <sup>IV</sup>B (Marschall et al. 2004). Kalt et al. (2001) pointed out that the main substitutions (in the series schorl-dravite to olenite) including <sup>IV</sup>B are most likely <sup>Y</sup>Al<sup>3+</sup> + <sup>T</sup>B<sup>3+</sup> = <sup>T</sup>Si<sup>4+</sup> + <sup>Y</sup>(Mg,Fe)<sup>2+</sup>, which is a modified Tschermak's substitution. Hughes et al. (2004) showed that the presence of substantial <sup>IV</sup>B is limited to, or more common in, Al-rich tourmalines, and that the recent discoveries of <sup>IV</sup>B-bearing tourmalines imply that the assumption of ideal B stoichiometry is not valid for the more widespread elbaite-schorl-rossmanite tourmalines, and the B content must be measured.

Hence, it was of interest to determine whether tourmaline from the liddicoatite-elbaite series could also contain <sup>IV</sup>B and how it is correlated to X-site and Y-site occupancy. We also wished to determine whether the vacancies reported at the Y site in Al-rich tourmalines are real or artifacts of the chemical and/or structural data. In this study, we characterize nearly colorless tourmalines (of the liddicoatite-elbaite series) from Anjanabonoina, Madagascar, by crystal-structure refinement and by chemical analyses (EMPA and SIMS). Previous investigations did not seek <sup>IV</sup>B in tourmalines from Madagascar, although the chemistry of this tourmaline had been studied in detail. History, mining, location, geology, associated minerals, chemical data, and properties of liddicoatite from Anjanabonoina, Madagascar, are summarized by Dirlam et al. (2002). This publication should be considered an addition to the extensive study and compilation by Dirlam et al. (2002) regarding liddicoatite from Anjanabonoina, Madagascar.

### REGIONAL GEOLOGY

The western part of Madagascar consists mostly of Mesozoic sedimentary rocks, whereas the central and eastern part is formed mainly of metamorphic and igneous rocks of the Mozambique orogenic belt (Petters 1991). The Mozambique orogenic belt was affected by tectonic activity, metamorphism, and plutonism from at least 950 Ma to about 450 Ma during the Pan-African orogeny (Petters 1991). Between 570 and 455 Ma the last magmatic cycle of the Pan-African orogeny generated granitic plutons and associated pegmatite fields. The gem-bearing pegmatites postdate the main tectonic phase and, therefore, are thought to be intruded during a late phase of the magmatic cycle.

Like many other gem-bearing pegmatites of Madagascar, the Anjanabonoina aplite-pegmatite field is situated in the Irempo Group, which consists of a lower unit of gneisses and an upper unit of quartzites, schists, and marbles (Pezzotta and Franchi 1997; Fernandez et al. 2001). The pegmatites were emplaced in a complex geologic environment, perhaps at the contact between the lower and upper unit. The aplite-pegmatite field extends for about 2.5 km. The veins are 2 to 12 m in thickness and large parts are kaolinized and/or deeply weathered (De Vito 2002). The Anjanabonoina pegmatites

contain quartz, microcline, albite, dravite-elbaite-liddicoatite tourmaline, spodumene, native bismuth, spessartine, beryl (morganite), hambergite, danburite, phenakite, and scapolite (De Vito 2002). Based on this mineral assemblage, they show characteristics intermediate between Li-Cs-Ta (LCT) and rare earth type (NYF) families of the rare-element and miarolitic classes (Černý 1991; Pezzotta 2001a).

## EXPERIMENTAL DETAILS

### Sample selection

Ten nearly colorless tourmaline crystals from pockets from Anjanabonoina, Madagascar, were investigated by energy dispersive spectrometry (EDS) and wavelength dispersive spectrometry (WDS) by electron-microprobe analyses (EMPA). The samples with the highest Al content, the lowest Si, Mn, and Fe contents, and with different Na/Ca ratios were subsequently chosen for structural investigation and chemical characterization by EMPA and SIMS. Sample LC1 was taken from the colorless rim [~3 mm thick; material from this rim was also taken for an ICP-MS analysis (LC1X)] of a tourmaline with a black (Fe-rich) core (~2 cm in diameter); the whole crystal is ~4 cm in diameter. Sample LID52 is from the very-light-pink intermediate zone (~4 mm thick) of a zoned crystal ~4 cm in diameter. Sample LID6A1 is from a colorless to very-light-pink intermediate zone (3 mm thick, near the rim), from a strongly zoned crystal ~15 cm in diameter. Sample LID3NEW is from a light-pink intermediate zone (~1 cm) of a tourmaline ~10 cm in diameter. To compare sample LC1X with chemically similar tourmalines by ICP-MS, sample AFGANT was taken from a colorless elbaite crystal (~9 mm in diameter), which grew in a pocket on quartz and albite crystals, from Nuristan, Kunar Province, Afghanistan, and another sample (OLE) was taken from a colorless B-rich olenite crystal, intergrown with quartz, from Stoffhütte, Koralle, Styria, Austria (~7 mm in diameter; Ertl et al. 1997; Hughes et al. 2000).

### Crystal-structure refinement

The tourmaline crystals were mounted on a Bruker Apex CCD diffractometer equipped with graphite-monochromated MoK $\alpha$  radiation. Refined cell-parameters and other crystal data are listed in Table 1. Redundant data were collected for an approximate sphere of reciprocal space, and were integrated and corrected for Lorentz and polarization factors using the Bruker program SAINTPLUS (Bruker AXS Inc. 2001).

The structure was refined using a tourmaline starting model and the Bruker SHELXTL v. 6.10 package of programs, with neutral-atom scattering factors and terms for anomalous dispersion. For H1, the hydrogen atom associated with O1, the O1-H1 bond distance was constrained to be within one  $\sigma$  of 0.86, the expected bond distance as measured by X-ray diffractometry. In addition, the occupancy of

**TABLE 1.** Crystal data and results of structure refinement of tourmalines from the liddicoatite-elbaite series from Anjanabonoina, Madagascar

Space group:	<i>R</i> 3 <i>m</i>	
Unit-cell parameters (Å):		
	LID3NEW: <i>a</i> = 15.8322(3), <i>c</i> = 7.1034(3)	LID6A1: <i>a</i> = 15.8204(3), <i>c</i> = 7.0955(2)
	LID52: <i>a</i> = 15.8119(3), <i>c</i> = 7.0925(2)	LC1: <i>a</i> = 15.8095(9), <i>c</i> = 7.0941(8)
Frame width, scan time, number of frames, detector distance:	0.20°, 15 s, 4500, 5 cm	
Measured reflections, full sphere:		
	LID3NEW: 10,936	LID6A1: 11,283
	LID52: 11,120	LC1: 11,145
Unique reflections; refined parameters:		
	LID3NEW: 1,105; 98	LID6A1: 1,094; 98
	LID52: 1,097; 98	LC1: 1,099; 98
<i>R</i> 1:		
	LID3NEW: 0.0165	LID6A1: 0.0147
	LID52: 0.0129	LC1: 0.0133
Difference peaks (+,-):		
	LID3NEW: 0.64, -0.26	LID6A1: 0.48, -0.27
	LID52: 0.34, -0.18	LC1: 0.38, -0.20
Goodness-of-Fit:		
	LID3NEW: 1.100	LID6A1: 1.122
	LID52: 1.122	LC1: 1.155

H1 was released (occupancy not fixed at 1.00). Refinement was performed with anisotropic thermal parameters for all non-hydrogen atoms. The atom parameters and interatomic distances are presented in Tables 2 and 3, respectively.

**TABLE 2.** Table of atom parameters in tourmalines from the liddicoatite-elbaite series from Anjanabonoina, Madagascar

Atom	x	y	Z	$U_{eq}$	refined occ.*
<b>LID3NEW:</b>					
X	0	0	$\frac{3}{4}$	0.0069(3)	Na <sub>1.349(8)</sub>
T	-0.19203(3)	-0.19009(3)	-0.01194(14)	0.00557(13)	Si <sub>0.950(5)</sub> B <sub>0.050</sub>
B	-0.10891(8)	2x	-0.4668(3)	0.0082(4)	B <sub>1.00</sub>
Y	-0.12340(8)	1/2x	0.3518(2)	0.0104(4)	Al <sub>0.576(4)</sub>
Z	-0.29675(3)	-0.25965(3)	0.37670(15)	0.00810(11)	Al <sub>1.00</sub>
O1	0	0	0.2026(5)	0.0365(10)	O <sub>1.00</sub>
O2	-0.05989(6)	2x	-0.4938(3)	0.0191(4)	O <sub>1.00</sub>
O3	-0.26830(13)	1/2x	0.4783(3)	0.0129(3)	O <sub>1.00</sub>
O4	-0.09253(6)	2x	-0.0866(2)	0.0106(3)	O <sub>1.00</sub>
O5	-0.18439(12)	1/2x	-0.1081(2)	0.0109(3)	O <sub>1.00</sub>
O6	-0.19564(8)	-0.18583(8)	0.2123(2)	0.0097(2)	O <sub>1.00</sub>
O7	-0.28612(7)	-0.28547(7)	-0.09272(19)	0.00845(19)	O <sub>1.00</sub>
O8	-0.20964(8)	-0.27022(8)	-0.4530(2)	0.0098(2)	O <sub>1.00</sub>
H1 (W)	-0.0552(10)	1/2x	0.151(8)	0.000(16)	H <sub>0.43(6)</sub>
H3 (V)	-0.267(3)	1/2x	-0.419(7)	0.041(12)	H <sub>1.00</sub>
<b>LID6A1:</b>					
X	0	0	$\frac{1}{4}$	0.0093(3)	Na <sub>1.198(7)</sub>
T	0.19196(2)	0.19000(2)	0.01538(14)	0.00611(12)	Si <sub>0.949(4)</sub> B <sub>0.051</sub>
B	0.10895(7)	2x	0.4698(3)	0.0082(3)	B <sub>1.00</sub>
Y	0.12266(7)	1/2x	-0.3470(2)	0.0104(3)	Al <sub>0.620(4)</sub>
Z	0.29675(3)	0.25979(3)	-0.37409(15)	0.00827(10)	Al <sub>1.00</sub>
O1	0	0	-0.2009(4)	0.0325(7)	O <sub>1.00</sub>
O2	0.05996(5)	2x	0.4991(3)	0.0188(3)	O <sub>1.00</sub>
O3	0.26689(12)	1/2x	-0.4759(2)	0.0138(2)	O <sub>1.00</sub>
O4	0.09279(5)	2x	0.0900(2)	0.0112(2)	O <sub>1.00</sub>
O5	0.18494(10)	1/2x	0.1115(2)	0.0117(2)	O <sub>1.00</sub>
O6	0.19538(6)	0.18539(7)	-0.2093(2)	0.00974(17)	O <sub>1.00</sub>
O7	0.28627(6)	0.28561(6)	0.09517(18)	0.00873(16)	O <sub>1.00</sub>
O8	0.20955(7)	0.27011(7)	0.45548(18)	0.00982(17)	O <sub>1.00</sub>
H1 (W)	0.0538(17)	1/2x	-0.145(6)	0.000(12)	H <sub>0.49(5)</sub>
H3 (V)	0.263(3)	1/2x	0.413(6)	0.049(11)	H <sub>1.00</sub>
<b>LID52:</b>					
X	0	0	$\frac{1}{4}$	0.0110(3)	Na <sub>1.094(6)</sub>
T	0.19188(2)	0.18990(2)	0.01696(14)	0.00605(11)	Si <sub>0.941(4)</sub> B <sub>0.059</sub>
B	0.10895(6)	2x	0.4713(3)	0.0083(3)	B <sub>1.00</sub>
Y	0.12240(6)	1/2x	-0.34536(19)	0.0102(3)	Al <sub>0.651(4)</sub>
Z	0.29674(2)	0.25991(2)	-0.37294(15)	0.00815(9)	Al <sub>1.00</sub>
O1	0	0	-0.2007(4)	0.0303(6)	O <sub>1.00</sub>
O2	0.05999(5)	2x	0.5022(2)	0.0183(3)	O <sub>1.00</sub>
O3	0.26596(10)	1/2x	-0.4746(2)	0.0138(2)	O <sub>1.00</sub>
O4	0.09304(5)	2x	0.0913(2)	0.0113(2)	O <sub>1.00</sub>
O5	0.18534(9)	1/2x	0.1129(2)	0.0118(2)	O <sub>1.00</sub>
O6	0.19522(6)	0.18508(6)	-0.20791(19)	0.00971(15)	O <sub>1.00</sub>
O7	0.28630(6)	0.28569(5)	0.09613(18)	0.00872(15)	O <sub>1.00</sub>
O8	0.20954(6)	0.27009(6)	0.45660(18)	0.00976(16)	O <sub>1.00</sub>
H1 (W)	0.0543(17)	1/2x	-0.146(6)	0.000(12)	H <sub>0.45(5)</sub>
H3 (V)	0.263(3)	1/2x	0.418(6)	0.052(10)	H <sub>1.00</sub>
<b>LC1:</b>					
X	0	0	$\frac{1}{4}$	0.0138(4)	Na <sub>1.014(7)</sub>
T	0.19165(2)	0.18970(2)	0.01911(18)	0.00651(11)	Si <sub>0.925(4)</sub> B <sub>0.075</sub>
B	0.10909(7)	2x	0.4732(3)	0.0083(3)	B <sub>1.00</sub>
Y	0.12250(6)	1/2x	-0.3432(2)	0.0099(3)	Al <sub>0.665(4)</sub>
Z	0.29678(2)	0.26009(3)	-0.37143(18)	0.00846(9)	Al <sub>1.00</sub>
O1	0	0	-0.2009(4)	0.0275(6)	O <sub>1.00</sub>
O2	0.06001(5)	2x	0.5064(3)	0.0173(3)	O <sub>1.00</sub>
O3	0.26455(11)	1/2x	-0.4729(2)	0.0146(2)	O <sub>1.00</sub>
O4	0.09329(5)	2x	0.0932(2)	0.0118(2)	O <sub>1.00</sub>
O5	0.18584(10)	1/2x	0.1146(2)	0.0122(2)	O <sub>1.00</sub>
O6	0.19487(6)	0.18469(6)	-0.2058(2)	0.00993(16)	O <sub>1.00</sub>
O7	0.28619(6)	0.28565(6)	0.0973(2)	0.00912(16)	O <sub>1.00</sub>
O8	0.20959(6)	0.27011(6)	0.4580(2)	0.00986(17)	O <sub>1.00</sub>
H1 (W)	0.0529(19)	1/2x	0.140(6)	0.000(13)	H <sub>0.44(5)</sub>
H3 (V)	0.262(3)	1/2x	0.423(6)	0.047(10)	H <sub>1.00</sub>

\* Optimized occupancies in Table 6.

## Chemical analyses

After completion of the structure refinement, the four crystals selected for crystal structure determination were mounted in plugs and polished for chemical analysis. All elements (except B, Li, Be, and H) were determined with a Cameca SX51 electron microprobe (EMP) equipped with five wavelength-dispersive spectrometers (Universität Heidelberg). Operating conditions were 15 kV accelerating voltage, 20 nA beam current, and a beam diameter of 5  $\mu$ m. Peaks for all elements were measured for 10 s, except for Mg (20 s), Cr (20 s), Ti (20 s), Zn (30 s), and F (40 s). Natural and synthetic silicate and oxide standards were used for calibration (Ertl et al. 2003). The analytical data were reduced and corrected using the PAP routine. A modified matrix correction was applied assuming stoichiometric O atoms and all non-measured components as B<sub>2</sub>O<sub>3</sub>. Accuracy of the electron-microprobe analyses and correction procedure were checked by measuring three reference tourmalines (98114: elbaite, 108796: dravite, 112566: schorl). Compositions of these tourmaline samples are presented in the context of an interlaboratory comparison study (Dyar et al. 1998, 2001). Agreement between the published analyses and the measured values was good. Under the described conditions, analytical errors on all analyses are  $\pm 1\%$  relative for major elements and  $\pm 5\%$  relative for minor elements.

Hydrogen, Be, Li, and B were determined by secondary ion mass spectrometry (SIMS) with a CAMECA ims 3f ion microprobe (Universität Heidelberg). Primary O-ions were accelerated to 10 keV. The energy window of the mass spectrometer was set to 40 eV. An offset of 75 V was applied to the secondary accelerating voltage of 4.5 kV so that secondary ions with an initial energy of 75  $\pm 20$  eV were analyzed (energy filtering). This adjustment suppresses effects of light elements related to the matrix (Ottolini et al. 1993). For B, Be, and Li, the primary current was 20 nA, resulting in a sputtering surface  $\sim 30 \mu$ m in diameter. The spectrometer's mass resolution ( $M/\Delta M$ ) for B, Be, and Li was set to  $\sim 1100$  (10%) to suppress interferences ( $^6\text{LiH}^+$ ,  $^{10}\text{BH}^+$ ,  $\text{Al}^{3+}$ ). Secondary ions  $^7\text{Li}$ ,  $^9\text{Be}$ , and  $^{11}\text{B}$  were collected under an ion-imaged field of 150  $\mu$ m diameter.

For H, the primary beam current was 25 nA and  $M/\Delta M$  was set to  $\sim 400$  (10%). To reduce the rate of contamination with water, a smaller field aperture was chosen (Marschall and Ludwig 2004); thus, the analyzed area was restricted to 10  $\mu$ m in diameter in the center of the scanned area. This method reduces the influx of water into the vacuum chamber, which was found to be higher on the edge of the primary beam spot than in the center. Water contamination was further reduced using a liquid

**TABLE 3.** Selected interatomic distances in tourmalines from the liddicoatite-elbaite series from Anjanabonoina, Madagascar

	LID3NEW	LID6A1	LID52	LC1
<b>X-</b>				
O2 $\times$ 3	2.386(2)	2.413(2)	2.429(1)	2.451(2)
O5 $\times$ 3	2.722(2)	2.718(1)	2.718(1)	2.720(1)
O4 $\times$ 3	2.790(2)	2.785(1)	2.786(1)	2.786(1)
Mean	2.649	2.639	2.644	2.652
<b>Y-</b>				
O1	1.997(2)	1.975(2)	1.965(1)	1.958(2)
O2 $\times$ 2	1.996(1)	1.989(1)	1.981(1)	1.974(1)
O6 $\times$ 2	1.976(1)	1.968(1)	1.964(1)	1.959(1)
O3	2.180(2)	2.177(2)	2.169(2)	2.152(2)
Mean	2.020	2.011	2.004	1.996
<b>Z-</b>				
O7	1.887(1)	1.8850(9)	1.8839(8)	1.8848(9)
O8	1.884(1)	1.8833(9)	1.8831(8)	1.8825(9)
O6	1.850(1)	1.854(1)	1.8567(9)	1.8648(9)
O8'	1.904(1)	1.9020(9)	1.9002(8)	1.8997(9)
O7'	1.958(1)	1.9518(9)	1.9480(8)	1.9455(9)
O3	1.9434(8)	1.9482(7)	1.9513(6)	1.9575(7)
Mean	1.904	1.904	1.904	1.906
<b>T-</b>				
O7	1.6057(10)	1.6055(9)	1.6053(8)	1.6048(8)
O6	1.5965(10)	1.5975(10)	1.5989(9)	1.5990(10)
O4	1.6261(6)	1.6239(5)	1.6216(5)	1.6186(5)
O5	1.6417(7)	1.6391(6)	1.6366(6)	1.6334(6)
Mean	1.6175	1.6165	1.6156	1.6140
<b>B-</b>				
O2	1.358(3)	1.358(2)	1.359(2)	1.365(2)
O8 ( $\times$ 2)	1.385(1)	1.382(1)	1.382(1)	1.380(1)
Mean	1.376	1.374	1.374	1.375

nitrogen coldtrap attached to the sample chamber of the ims 3f.

The count rates of the analyzed isotopes ( $^7\text{Li}$ ,  $^9\text{Be}$ , and  $^{11}\text{B}$ ) were normalized to the count rate of  $^{30}\text{Si}$ . The ion yield (RIY) of B and H relative to Si was determined using three different reference tourmalines: elbaite (98144), dravite (108796), and schorl (112566), all described and analyzed by Dyar et al. (1998, 2001). The reference material for Li and Be was the SRM610 NIST standard glass with concentrations for Li and Be published by Pearce et al. (1997). The relative reproducibility ( $1\sigma$ ) for the RIY of B, Li, and Be was  $<1\%$ . Matrix effects and the uncertainty of the element concentrations in the reference material limit the accuracy of the analysis. The relative uncertainty is estimated to be  $<20\%$  for Li and  $<10\%$  for B. The relative uncertainty is estimated to be  $<10\%$  for H by comparison of seven tourmalines with different compositions and from different localities (Ertl et al. 2004a; M. Darby Dyar unpublished data), which have also been measured by U-extraction (Dyar et al. 1998). Table 4 contains complete chemical analyses for the tourmaline samples from Anjanabonoina, Madagascar.

The sample preparation for the ICP-MS analyses of the tourmaline samples LC1X and AFGANT was performed in a clean-laboratory using ultrapure acids. To remove surface contamination, the tourmaline grains were leached in 2.5 n HCl for 15 minutes at about  $80^\circ\text{C}$ . Chemical sample digestion was performed in tightly sealed Teflon beakers using a HF/HClO<sub>4</sub> mixture of 5:1. After about 3 months at  $100^\circ\text{C}$ , the samples were evaporated and transformed into chlorides using HCl and finally into nitrates using HNO<sub>3</sub>. ICP-MS analyses were performed on an ELAN 6100 (Perkin Elmer / SCIEX; at the Geozentrum, Universität Wien). Table 5 contains chemical data from the ICP-MS analyses.

## Infrared spectra

Infrared spectra were collected on Nicolet Nexus FTIR spectrometer (at the National Geophysical Research Institute, Hyderabad) equipped with TEC-DTGS detector and a XT-KBr beam splitter. The spectrometer has a dual source covering a  $375$  to  $11000\text{ cm}^{-1}$  wavenumber range. Thin plates ( $\sim 1 \times \sim 1 \times 0.700\text{ mm}$  in size) were cut off the colorless rim of tourmaline LC1 and were heated at  $\sim 80^\circ\text{C}$  for about 3 h before collecting the IR spectra. A circular aperture (of the same size as the plate) was just covered by the thin plate, and the spectrum was recorded in the range  $2000$ – $11000\text{ cm}^{-1}$ . This spectrum was recorded with unpolarized light (no wire-grid polarizer was available), covering overtone and combination modes in the range  $3000$ – $6000\text{ cm}^{-1}$ .

## RESULTS AND DISCUSSION

### Crystal structure

Because the T-site occupancies exceed 6.00 apfu in the range 6.07–6.16 (Table 4), B<sub>2</sub>O<sub>3</sub> in the optimized formulae was calculated as  $9.00 - \text{Si (apfu)} = \text{B (apfu)}$  (iterated until the calculated SiO<sub>2</sub> value was identical with the measured value), and OH was calculated as  $4.00 - \text{F (apfu)} = \text{OH (apfu)}$  (Table 4). Using this method, the structural formulae of these tourmaline samples are:

**TABLE 4.** Composition of tourmalines from the liddicoatite-elbaite series from Anjanabonoina, Madagascar (wt%)

	LID3NEW*†	LID3NEW‡	LID6A1*†	LID6A1‡	LID52*†	LID52‡	LC1*†	LC1‡
SiO <sub>2</sub>	37.34	37.34	36.63	36.63	36.38	36.38	35.70	35.70
TiO <sub>2</sub>	0.01	–	0.02	–	0.01	–	0.04	–
B <sub>2</sub> O <sub>3</sub>	12.40	11.60	12.56	12.09	12.98	12.29	13.45	12.80
Al <sub>2</sub> O <sub>3</sub>	39.62	40.07	40.79	40.92	41.77	41.38	42.64	42.62
FeO§	0.01	–	0.35	0.35	0.18	0.18	0.10	0.10
MnO§	0.52	0.52	0.14	0.14	0.31	0.31	0.08	0.08
MgO	0.00	–	0.00	–	0.00	–	0.01	–
CaO	3.43	3.43	2.98	2.98	2.44	2.44	1.78	1.78
Li <sub>2</sub> O	2.10	2.10	1.82	1.82	1.73	1.73	1.42	1.42
ZnO	0.03	–	0.01	–	0.01	–	0.01	–
Na <sub>2</sub> O	0.96	0.96	1.13	1.13	1.35	1.35	1.54	1.54
K <sub>2</sub> O	0.01	–	0.01	–	0.01	–	0.01	–
F	1.53	1.53	1.13	1.13	1.03	1.03	1.02	1.02
H <sub>2</sub> O	3.06	3.10	3.30	3.29	3.02	3.35	3.51	3.37
O=F	–0.64	–0.65	–0.48	–0.48	–0.43	–0.44	–0.43	–0.43
Sum	100.38	100.00	100.39	100.00	100.79	100.00	100.88	100.00
N	31	31	31	31	31	31	31	31
Si	5.82	5.86	5.70	5.73	5.65	5.69	5.50	5.56
<sup>11</sup> B	0.34	0.14	0.38	0.27	0.48	0.31	0.57	0.44
Sum T site	6.16	6.00	6.08	6.00	6.13	6.00	6.07	6.00
<sup>13</sup> B	3.00	3.00	3.00	3.00	3.00	3.00	3.00	3.00
Al	7.28	7.41	7.49	7.55	7.64	7.62	7.73	7.82
Mn <sup>2+</sup>	0.07	0.07	0.02	0.02	0.04	0.04	0.01	0.01
Fe <sup>2+</sup>	–	–	0.05	0.05	0.02	0.02	0.01	0.01
Li	1.32	1.33	1.14	1.15	1.08	1.09	0.88	0.89
Sum Y, Z sites	8.67	8.81	8.70	8.77	8.78	8.77	8.63	8.73
Ca	0.57	0.58	0.50	0.50	0.41	0.41	0.29	0.30
Na	0.29	0.29	0.34	0.34	0.41	0.41	0.46	0.46
□	0.14	0.13	0.16	0.16	0.18	0.18	0.25	0.24
Sum X site	1.00	1.00	1.00	1.00	1.00	1.00	1.00	1.00
Sum cations	18.69	18.68	18.62	18.61	18.73	18.59	18.45	18.49
OH	3.18	3.24	3.43	3.44	3.13	3.49	3.60	3.50
F	0.75	0.76	0.56	0.56	0.51	0.51	0.50	0.50
Sum OH + F	3.93	4.00	3.99	4.00	3.64	4.00	4.10	4.00

\* Average of 12 EMP analyses for sample LID3NEW, 15 EMP analyses for sample LID6A1, 10 EMP analyses for sample LID52, and 20 EMP analyses for sample LC1.

† Average of 3 SIMS analyses for B<sub>2</sub>O<sub>3</sub>, Li<sub>2</sub>O, and BeO, and 2 SIMS analyses for H<sub>2</sub>O for sample LID3NEW; 5 SIMS analyses for B<sub>2</sub>O<sub>3</sub>, Li<sub>2</sub>O, and BeO, and 3 SIMS analyses for H<sub>2</sub>O for samples LID6A1 and LID52; 3 SIMS analyses for B<sub>2</sub>O<sub>3</sub>, Li<sub>2</sub>O, and BeO and 1 SIMS analysis for H<sub>2</sub>O for sample LC1. For samples LID3NEW and LID52 BeO = 26 ppm, for sample LID6A1 BeO = 28 ppm, and for sample LC1 BeO = 19 ppm.

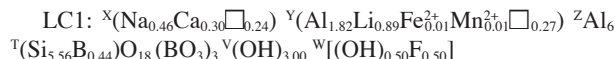
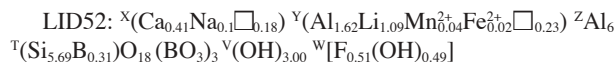
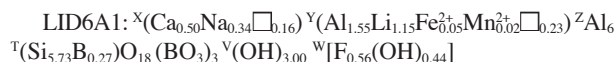
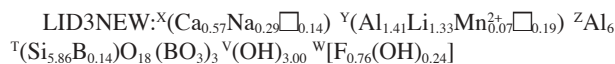
‡ Weight percent calculated for an optimized formula, where B<sub>2</sub>O<sub>3</sub> was calculated as  $9.00 - \text{Si (apfu)} = \text{B (apfu)}$  (iterated till the calculated SiO<sub>2</sub> value was identical with the measured value), OH was calculated as  $4.00 - \text{F (apfu)} = \text{OH (apfu)}$ ; Al<sub>2</sub>O<sub>3</sub> was slightly corrected ( $\leq 1\%$ ) for a total sum of 100%, because Al<sub>2</sub>O<sub>3</sub> is the component with the highest amounts in all samples, hence the absolute error is believed to be here more significant than for other oxides.

§ Total Mn and total Fe calculated as MnO and FeO. Cl and Cr are below the detection limit in all samples.

**TABLE 5.** Chemical data determined by ICP-MS analyses of colorless elbaite from Anjanabonoina, Madagascar (LC1X), and from Nuristan, Afghanistan (AFGANT) (oxides in wt%, elements in ppm)

	LC1X	AFGANT	OLE		LC1X	AFGANT	OLE
Al <sub>2</sub> O <sub>3</sub>	41.55	41.56	–	Pb	550	97	99
FeO	0.18	0.03	–	Bi	25	1.0	0.55
CaO	2.15	1.24	–	Th	4.4	3.3	1.1
MgO	0.01	<0.01	–	U	0.028	0.21	0.28
Na <sub>2</sub> O	1.56	1.70	–				chondrite
K <sub>2</sub> O	0.01	0.01	–	La	47.2	12.5	3.5
MnO	0.14	0.55	–	Ce	71	22.9	8.3
TiO <sub>2</sub>	0.06	0.03	–	Pr	6.3	2.2	0.88
P <sub>2</sub> O <sub>5</sub>	0.024	0.010	0.03	Nd	18.6	5.7	3.1
Li <sub>2</sub> O	2.00	2.15	–	Sm	3.6	1.9	1.0
Be	18.6	20.0	37.0	Eu	0.575	0.019	0.092
Cr	5.1	2.2	–	Gd	4.0	1.5	0.97
Co	0.3	0.32	0.5	Tb	0.2	0.12	0.10
Ni	0.8	<1	66	Dy	0.56	0.36	0.44
Rb	0.65	0.8	27	Ho	0.047	0.017	0.068
Sr	273	10.3	189	Er	0.20	0.061	0.22
Cs	2.2	1.7	5.0	Tm	0.009	<0.005	0.031
Ba	7.6	5.5	43	Yb	0.091	0.02	0.24
Sc	139	3.5	1.8	Lu	0.023	0.004	0.031
Y	2.1	1.0	2.2	ΣREE	152.4	70.2	19.0

Notes: Chondrite values compiled by T. Meisel from Raith et al. (2004) (all REE exclusive of Ho and Er; Wasson and Kallemeyn 1988; Ho: McDonough and Sun 1995; Er: Palme 1988). Dashes: not analyzed.



Similar results were obtained by using the optimization method of Wright et al. (2000), a method where the optimized formula essentially minimizes the differences between the formula obtained from the results of the chemical analysis and that obtained by single-crystal structure refinement (SREF).

The structure refinements show significant amounts of <sup>IV</sup>B (~0.30–0.45 apfu), and the <T-O> bond-lengths (~1.618–1.614 Å; Table 3) reflect that substitution of <sup>IV</sup>B. All investigated samples from Madagascar clearly show excess B by SIMS. The SIMS derived B<sub>2</sub>O<sub>3</sub> values are 5.5 ± 1.5% too high compared to the recalculated B<sub>2</sub>O<sub>3</sub> values from the optimized formulae. The refined values for <sup>IV</sup>B (Table 2) are in good agreement with the values from the optimized formulae (within 2–15%). Only sample LID3NEW shows a value for <sup>IV</sup>B significantly higher (~0.30 apfu; Table 2) than the optimized formula (~0.14 apfu; Table 4). Possible explanations are that relatively small amounts of <sup>IV</sup>B cannot be estimated by refinement very accurately. Figure 1 shows the correlation between the <sup>IV</sup>B (from the optimized formulae by using only chemical data from Table 4), and the <T-O> bond-lengths ( $r^2 = 0.9838$ ). It is increasingly clear that the <sup>IV</sup>B ↔ <sup>IV</sup>Si substitution in tourmaline is not rare, and the liddicoatite-elbaite series also displays that substitution. The amount of <sup>IV</sup>B increases with increasing Na content in these tourmalines,

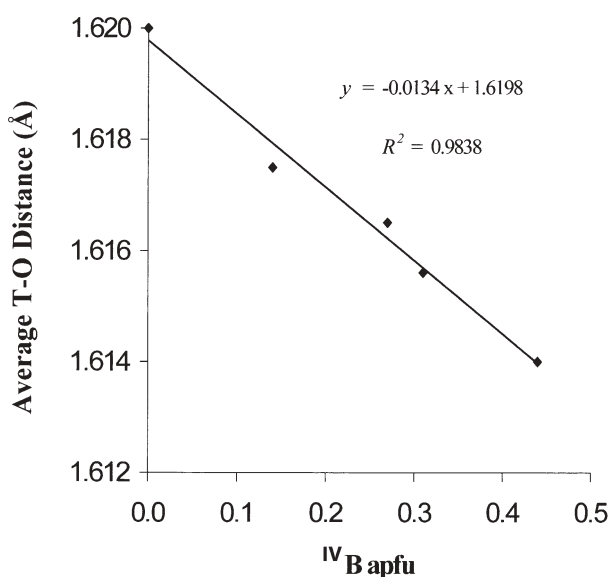


**FIGURE 1.** Relationship between the average T-O bond length (Å) and the amount of tetrahedrally coordinated boron (apfu) (from the optimized formulae). Graph includes the ideal bond length for a T site completely occupied by Si [ $\langle\text{T-O}\rangle \approx 1.620$  Å; MacDonald and Hawthorne 1995; Bloodaxe et al. 1999; Ertl et al. 2001; Bosi and Lucchesi 2004 (average value for all samples with Si 5.95–6.00 apfu)]. This correlation is valid for samples where the T site is only occupied by Si and B (no significant <sup>IV</sup>Al).

a correlation not yet reported from any other locality. In contrast, in the Fe-bearing olenites from the Korralpe, Austria, the amount of <sup>IV</sup>B increases with increasing Ca content. However, the X-site occupancy is not simply correlated with occupancy of <sup>IV</sup>B in the adjacent tetrahedral ring as was pointed out by Hughes et al. (2004). Similar to the Fe-bearing olenites from Korralpe, Austria (Hughes et al. 2004), the liddicoatite-elbaite samples from Madagascar also show a positive correlation between the Al occupation at the Y site (from the optimized formulae) and <sup>IV</sup>B (Fig. 2;  $r^2 = 0.9884$ ). We assume that for tourmaline samples from the liddicoatite-elbaite series, B should only be calculated as a stoichiometric constituent when these samples contain significant amounts of Mn and/or Fe (an intense color may be an indication). Iron- and/or Mn-poor, Al-rich (near colorless) tourmaline samples from the liddicoatite-elbaite series should only be calculated with a stoichiometric B content when the CaO content exceeds 3.5 wt%.

The structural (optimized) formulae of all investigated Li-rich tourmalines from Anjanabonoina, Madagascar, show  $\square_{0.19}$  to  $\square_{0.27}$  (vacancies) on the Y site (Table 4). The vacancies increase slightly with increasing Al content on the Y site. Other Al-rich and Li-bearing tourmalines (olenite) also have shown significant vacancies (~ $\square_{0.2}$ ) on the Y site (Ertl et al. 1997, 2004b; Hughes et al. 2000, 2004; Schreyer et al. 2002). We believe there is a short-range order configuration with  $(\text{Al}_2\square)$  at 3Y sites that is responsible for these vacancies (Table 6). We do not believe that these vacancies result from incorrect Li<sub>2</sub>O SIMS values because, in many samples, the Li content is relatively low. The most Li-poor sample from this investigation, LC1 (~0.9 apfu Li), yields

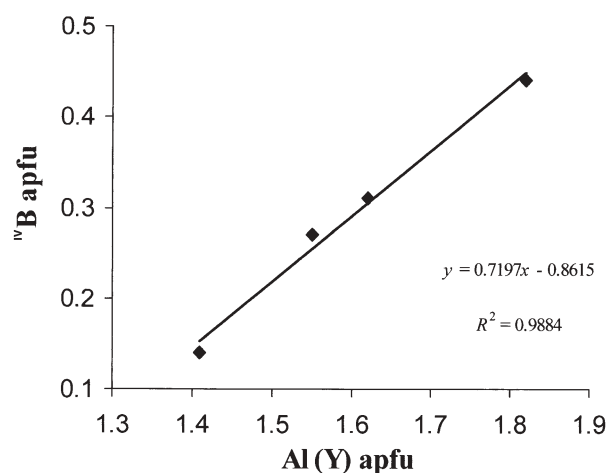


**FIGURE 2.** Relationship between the Al content at the Y site and <sup>10</sup>B (both from the optimized formulae) in tourmalines from the liddicoatite-elbaite series from Anjanabonoina, Madagascar (FeO + MnO ≤ 0.5 wt%).

□<sub>0.27</sub> in the optimized formula (Table 4). The olenite samples are indeed lower in Li and, therefore, the calculated Li<sub>2</sub>O content, assuming no vacancies at the Y site, is much too high (>30%) compared with the measured Li<sub>2</sub>O contents for these samples. Furthermore, the Y-site vacancies cannot be filled by Al because Al has significantly more electrons than Li, and hence the calculated electron occupancy would be much too high compared to the observed electron occupancy at the Y site. Additionally, it is clearly evident by checking the proportions of the short-range order configurations in Table 6 that the amount of <sup>10</sup>B is coupled with an occupancy of (Al<sub>2</sub>Li) [2.2] and (Al<sub>2</sub>□) [3.1] at the Y site, whereas the occupancy with (Li<sub>2</sub>Al) ([3.2]; liddicoatite end-member) requires the T site to be filled completely with Si. This correlation is an explanation for the increasing <sup>10</sup>B content with increasing Al content at the Y site (see Fig. 2). The calculated occupants (by using the short-range order configurations from Table 6) for all tourmaline samples are in very good agreement with the optimized formulae (Tables 4 and 6). Because of these satisfactory results, we believe that these proposed short-range order configurations mirror the real occupancies. We, thus, conclude that calculation of the Li content by filling the Y site completely with Li when no chemical analysis is available is problematic for Al-rich (and Li-bearing) tourmalines.

OH and F could, in principle, occur at the V site (O3 site) and W site (O1 site) in these Li-rich tourmaline samples. In all these samples, H3 (the hydrogen site associated with O3) was easily located as the highest peak in the near-final difference-Fourier map, and the position and isotropic-displacement parameter refined without problem; thus O3 was assigned as OH. Also, a difference peak (between +0.6 to +0.8 e/Å<sup>3</sup>), distinctly larger than background, was found near O1, and hence that site was assigned to F and OH. Grice and Ercit (1993) showed, using bond-valence arguments, that F orders at the O1 site in a wide variety of tourmaline structures. MacDonald and Hawthorne (1995) refined the F-OH occupancy of the O1 site in nine samples of F-rich uvite. They noted that in the tourmaline structure, the O1 and O3 anions are generally monovalent, and hence, F potentially can

substitute for OH at either or both of these sites. A comparison of the refined F occupancy of O1 with the F content determined by EMPA is given in Figure 5 of MacDonald and Hawthorne (1995). These values indicate that F strongly to completely orders onto the O1 site in these uvite samples. Our experience shows that significant peaks associated with H1 (electron density in a distance of ~0.6 Å from O1) occur only in Li-bearing tourmaline samples. This association is in agreement with stable short-range order arrangements proposed by Hawthorne (2002) for tourmalines with (Li<sub>2</sub>Al) or (Al<sub>2</sub>Li) at the Y sites, obtained by using local bond-valence requirements. Because definitive assessment of the ordering of the isoelectronic species O<sup>2-</sup> (of an OH) and F<sup>-</sup> is beyond the limits of X-ray diffraction studies, we assign all F to the O1 site in our final formulae of the liddicoatite-elbaite samples from Madagascar based on the arguments of Grice and Ercit (1993). All liddicoatite-elbaite formulae can be explained very accurately by short-range order configurations where the W site (O1 site) is occupied by OH or F (Table 6). There is no need to include short-range order configurations where the W site is occupied by O<sup>2-</sup>. This is in agreement with the chemical analyses for these samples, where (OH) + F = 3.93–4.10 pfu (Table 4). Only sample LID52 shows a ~9.9% lower water content, which is still within the error on the H<sub>2</sub>O SIMS analysis. However, because electron density in a distance of ~0.6 Å from O1 (+0.6 e/Å<sup>3</sup>; reflects the H which is bound to O1) in sample LID52 is similar to that in LID6A1 and LC1, we believe that there are similar amounts of OH in this sample. Hence, in Li-rich tourmalines of the elbaite-liddicoatite series (without significant Mg, Mn, and Fe contents), the OH content most probably can be calculated as 4 – F = OH.

### OH and H<sub>2</sub>O

Figure 3 displays the FTIR spectrum of a B-rich elbaite-liddicoatite. The bands around 4600–4300 cm<sup>-1</sup> in Figure 3 are combinations due to OH stretch + MOH bends; the same bands around 7600–6700 cm<sup>-1</sup> are the overtones of OH stretching modes (Fig. 3). Figure 4 magnifies the OH stretching mode region. Akizuki et al. (2001) reported similar FTIR spectra on triclinic liddicoatite from a pegmatite in Jochy, Madagascar.

The near-IR spectra comprises three regions: (1) the high wavenumber region between 6400 and 7400 cm<sup>-1</sup> attributed to the first overtone of the fundamental hydroxyl-stretching mode; (2) the 4800–5400 cm<sup>-1</sup> region attributed to water combination modes of the hydroxyl fundamentals of water; and (3) the 4000–4800 cm<sup>-1</sup> region attributed to the combination of the stretching and deformation modes (Frost et al. 2000, 2005). Kovács et al. (2003) interpreted bands appearing in the 4700–5400 cm<sup>-1</sup> region as combinations of stretching and bending modes. Figure 3 shows a significant band at 5195 cm<sup>-1</sup> and a weaker mode at 5380 cm<sup>-1</sup> in tourmaline sample LC1. Bands at about 5200 cm<sup>-1</sup> result from the combination of stretching and bending modes of molecular water (e.g., Arredondo et al. 2001). Because it is not clear if H<sub>2</sub>O is present as fluid inclusions or as a part of the structure, particular care was taken in the spectroscopic experiments to distinguish between the two possibilities. The FTIR spectra of sample LC1 were recorded at different temperatures (27, 300, 500, and 600 °C; Figs. 5 and 6a). It can be seen from the Figure 5 that the two bands at 5195 and 5380 cm<sup>-1</sup> can be

**TABLE 6.** Possible short-range order configurations

X site	Y site	T site	W site	Proportion				Reference	
				LC1	LID52	LID6A1	LID3NEW		
[1.1]	□	Al <sub>2</sub> Li	Si <sub>6</sub>	OH	0.24	0.18	0.16	0.14	Selway et al. (1998); Hughes et al. (2000)
[2.1]	Na	Al <sub>2</sub> □	Si <sub>6</sub>	OH	0.13	0.13	0.11	0.13	Schreyer et al. (2002); Ertl et al. (2003)
[2.2]	Na	Al <sub>2</sub> Li	Si <sub>5</sub> B	F	0.31	0.22	0.16	0.09	Schreyer et al. (2002)
[2.3]	Na	AlFe <sup>2+</sup> Li	Si <sub>6</sub>	F	0.01	0.02	0.05	–	modified after Ertl et al. (2003)
[2.4]	Na	AlMn <sup>2+</sup> Li	Si <sub>6</sub>	F	0.01	0.04	0.02	0.07	Ertl et al. (2003)
[3.1]	Ca	Al <sub>2</sub> □	Si <sub>5</sub> B	OH	0.14	0.10	0.11	0.06	modified after Ertl et al. (2003)
[3.2]	Ca	Li <sub>2</sub> Al	Si <sub>6</sub>	F	0.16	0.31	0.39	0.51	modified after Dunn et al. (1977)

Notes: The Z site of all listed short-range order configurations is occupied by Al<sub>6</sub>. The Y site (O3 sites) is occupied by (OH)<sub>3</sub>. For short-range order [1.1] the W site was occupied with (OH) because Henry (2005) showed that a summary and evaluation of >560 tourmaline analyses from many different tourmaline varieties illustrates that in tourmalines with more than 0.5 X-site vacancies there is little or no F present in the tourmaline. All other short-range orders with Li at the Y site are assumed to have F at the W site.

Calculated occupants:

LC1: X = (Na<sub>0.46</sub>Ca<sub>0.30</sub>□<sub>0.24</sub>) Y = (Al<sub>1.82</sub>Li<sub>0.89</sub>Fe<sub>0.01</sub>Mn<sub>0.01</sub>□<sub>0.27</sub>) T = (Si<sub>5.55</sub>B<sub>0.45</sub>) W = [(OH)<sub>0.51</sub>F<sub>0.49</sub>]  
 LID52: X = (Ca<sub>0.41</sub>Na<sub>0.41</sub>□<sub>0.18</sub>) Y = (Al<sub>1.63</sub>Li<sub>1.08</sub>Mn<sub>0.04</sub>Fe<sub>0.02</sub>□<sub>0.23</sub>) T = (Si<sub>5.68</sub>B<sub>0.32</sub>) W = [F<sub>0.59</sub>(OH)<sub>0.41</sub>]  
 LID6A1: X = (Ca<sub>0.50</sub>Na<sub>0.34</sub>□<sub>0.16</sub>) Y = (Al<sub>1.54</sub>Li<sub>1.17</sub>Fe<sub>0.05</sub>Mn<sub>0.02</sub>□<sub>0.22</sub>) T = (Si<sub>5.73</sub>B<sub>0.27</sub>) W = [F<sub>0.62</sub>(OH)<sub>0.38</sub>]  
 LID3NEW: X = (Ca<sub>0.57</sub>Na<sub>0.29</sub>□<sub>0.14</sub>) Y = (Al<sub>1.42</sub>Li<sub>1.32</sub>Mn<sub>0.07</sub>□<sub>0.19</sub>) T = (Si<sub>5.85</sub>B<sub>0.15</sub>) W = [F<sub>0.67</sub>(OH)<sub>0.33</sub>]  
 optimized occupants (from Table 4):  
 LC1: X = (Na<sub>0.46</sub>Ca<sub>0.30</sub>□<sub>0.24</sub>) Y = (Al<sub>1.82</sub>Li<sub>0.89</sub>Fe<sub>0.01</sub>Mn<sub>0.01</sub>□<sub>0.27</sub>) T = (Si<sub>5.56</sub>B<sub>0.44</sub>) W = [(OH)<sub>0.50</sub>F<sub>0.50</sub>]  
 LID52: X = (Ca<sub>0.41</sub>Na<sub>0.41</sub>□<sub>0.18</sub>) Y = (Al<sub>1.62</sub>Li<sub>1.09</sub>Mn<sub>0.04</sub>Fe<sub>0.02</sub>□<sub>0.23</sub>) T = (Si<sub>5.69</sub>B<sub>0.31</sub>) W = [F<sub>0.51</sub>(OH)<sub>0.49</sub>]  
 LID6A1: X = (Ca<sub>0.50</sub>Na<sub>0.34</sub>□<sub>0.16</sub>) Y = (Al<sub>1.55</sub>Li<sub>1.15</sub>Fe<sub>0.05</sub>Mn<sub>0.02</sub>□<sub>0.23</sub>) T = (Si<sub>5.73</sub>B<sub>0.27</sub>) W = [F<sub>0.56</sub>(OH)<sub>0.44</sub>]  
 LID3NEW: X = (Ca<sub>0.57</sub>Na<sub>0.29</sub>□<sub>0.14</sub>) Y = (Al<sub>1.41</sub>Li<sub>1.33</sub>Mn<sub>0.07</sub>□<sub>0.19</sub>) T = (Si<sub>5.86</sub>B<sub>0.14</sub>) W = [F<sub>0.76</sub>(OH)<sub>0.22</sub>]

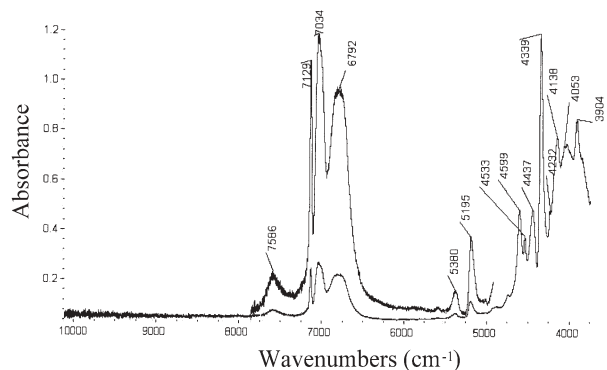


**FIGURE 3.** FTIR spectrum of B-rich elbaite-liddicoatite LC1 (random orientation). Accumulation of 2800 scans, with a resolution of 2 cm<sup>-1</sup>, sample thickness: 700 μm. The spectrum in the range 5000–8000 cm<sup>-1</sup> is the expanded version of the same figure with a maximum Y-scale of 0.3 (Absorbance).

observed up to 500 °C, and that they disappeared in the spectrum recorded at 600 °C. Upon cooling this sample (LC1) to 27 °C, these modes reappeared (Fig. 5). These variations are concomitant with progressive disappearance of hydroxyl bands observed at 4600–4300 and 7600–6700 cm<sup>-1</sup>, indicating that these two bands follow thermally induced variations in crystal structure. Moreover, we could not observe a significantly lower intensity of the bands 5195 and 5380 cm<sup>-1</sup> in the FTIR spectra upon cooling to 27 °C (Fig. 5). Additionally, if they are due to water inclusions, appearance of these spectral features should be spatially dependent; however, we observed similar spectra from five different crystal portions cut from a larger crystal. Our repeated experiments with different crystals gave similar spectral bands in this region, indicating that they may not be due to inclusions. As an additional check, the sample was cooled to -150 °C, and the bands could still be observed without significant spectral shifts (Fig. 5). In case of water as inclusions, they should normally freeze around -60 °C or lower (in the case of a two-phase inclusion) (Roedder 1984). However, the

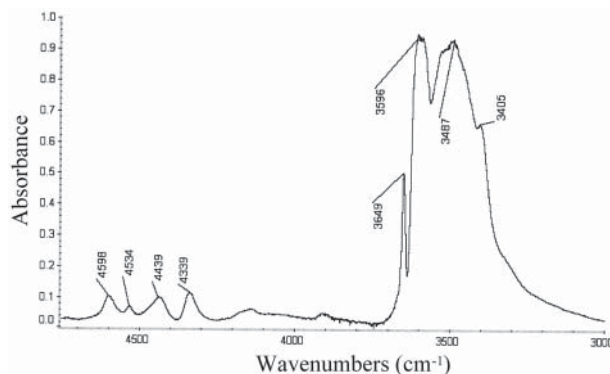


**FIGURE 4.** FTIR spectrum of B-rich elbaite-liddicoatite LC1 (random orientation). Accumulation of 1408 scans, with a resolution of 2 cm<sup>-1</sup>; sample thickness: ~10 μm.

spectrum at -150 °C is very similar to that recorded at 27 °C. In our experience, H<sub>2</sub>O fluid inclusions in quartz freeze at -25 °C (Prasad et al. 2006). Johnson and Rossman (2003) described an asymmetric band near 5200 cm<sup>-1</sup>, which is present in the near-IR spectra of the pegmatitic and metamorphic albite samples. This band resembles the combination stretch-bend mode for liquid water, and upon cooling to 77 K (~-200 °C) shifts to lower wavenumbers and resembles the near-IR spectrum of ice (Johnson and Rossman 2003). Hence, we conclude that these bands (~5195 and 5380 cm<sup>-1</sup>) in tourmaline sample LC1 cannot be explained by the presence of H<sub>2</sub>O in fluid inclusions. There is also a crystal-chemical possibility that H<sub>2</sub>O molecules could occur at the relatively large 9-coordinated X site. In fact, the B-rich elbaite-liddicoatite sample LC1 has the highest X-site vacancies (~□<sub>0.25</sub>) of all investigated tourmaline samples from Anjanabonoina. Similar bands ~5200 and ~5400 cm<sup>-1</sup> were previously observed in other tourmalines with vacancies at the X site (dravite-schorl sample from India; elbaite-schorl samples from different localities (G.R. Rossman, personal communica-

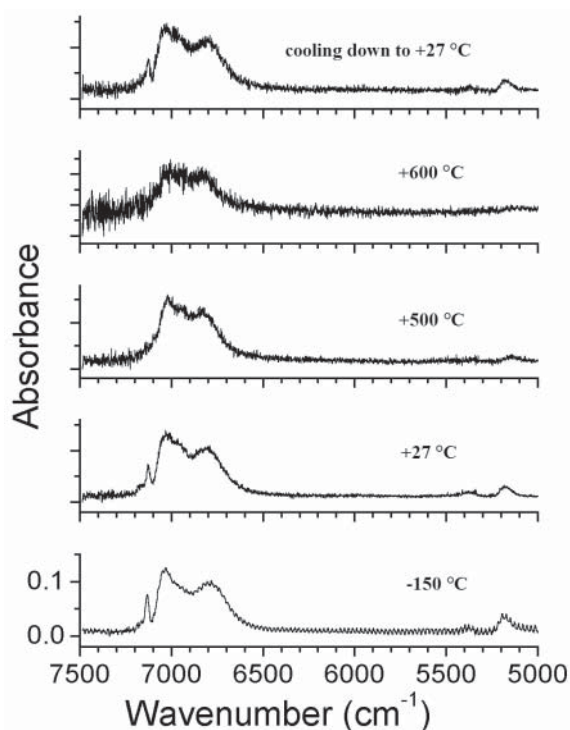


**FIGURE 5.** FTIR spectra of elbaite-liddicoatite LC1 at different temperatures:  $-150$ ,  $+27$ ,  $+500$ ,  $+600$ , and then back to  $+27$  °C (random orientation). Accumulation of 512 scans, with a resolution of  $2$   $\text{cm}^{-1}$ , sample thickness:  $700$   $\mu\text{m}$ .

tion 2005). Therefore, an additional FTIR spectrum was recorded from an Na-rich dravite (from Syros, Greece), with the formula  $\sim^{\text{X}}(\text{Na}_{1.0})^{\text{Y}}(\text{Mg}_{1.3}\text{Al}_{1.0}\text{Fe}_{0.4}^{2+}\text{Fe}_{0.2}^{3+}\text{Ti}_{0.1})^{\text{Z}}(\text{Al}_{4.9}\text{Mg}_{1.1})^{\text{T}}(\text{Si}_{5.8}\text{B}_{0.2})\text{O}_{18}(\text{BO}_3)_3^{\text{V}}(\text{OH})_{3.0}^{\text{W}}[(\text{OH})_{0.9}\text{F}_{0.1}]$  (Marschall et al. 2004) in which the X site is occupied completely by species other than  $\text{H}_2\text{O}$  in this sample. Interestingly, the FTIR spectrum from this Na-rich dravite does not show bands  $\sim 5200$  and  $\sim 5400$   $\text{cm}^{-1}$  (Fig. 6b).

Hence, it may be that small amounts of  $\text{H}_2\text{O}$  occur at the X site of pegmatitic tourmalines in which the site is not completely filled by Na, Ca, and K. The incorporation of molecular  $\text{H}_2\text{O}$  into the [001] structural channels of beryl (e.g., Wood and Nassau 1967, 1968; Pankrath and Langer 2002) is well documented, and we suggest here that  $\text{H}_2\text{O}$  may also occupy the tourmaline X site. Recently, Acosta-Vigil et al. (2002, 2003) have shown that the solubility of  $\text{H}_2\text{O}$  shows a positive correlation with the excess Al content of melt; they proposed that some  $\text{H}_2\text{O}$  may provide charge balance for excess Al. We suggest that future investigations of tourmalines that occur in late-stage igneous rocks and hydrothermal tourmalines (where the crystals are growing in aqueous solutions) consider the possibility of incorporation of  $\text{H}_2\text{O}$  molecules at the tourmaline X site.

#### Rare earth elements

Raith et al. (2004) noted that tourmaline is a significant carrier of REEs and therefore we also analyzed the REEs in our tourmaline samples. Chemical data determined by ICP-MS analyses of the colorless elbaite from Anjanabonoina, Mada-

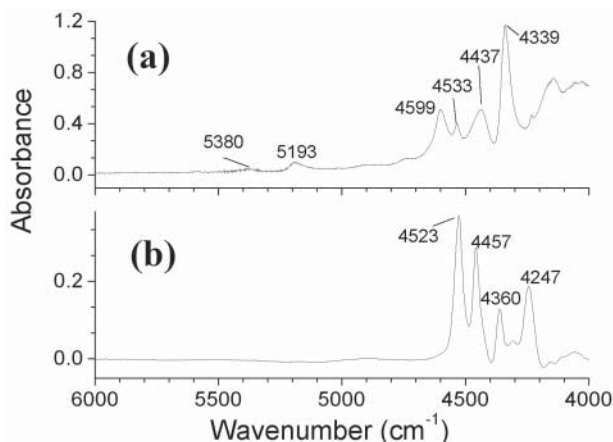


**FIGURE 6.** FTIR spectrum of (a) elbaite-liddicoatite LC1 ( $700$   $\mu\text{m}$  thick), from Anjanabonoina, Madagascar, and of (b) dravite SY309B ( $800$   $\mu\text{m}$  thick), from Syros, Greece (Marschall et al. 2004) (both in random orientation). Accumulation of 2800 scans, with a resolution of  $2$   $\text{cm}^{-1}$ . Spectra were taken at room temperature.

gascar (LC1X), a colorless elbaite from Nuristan, Afghanistan (AFGANT), with the optimized formula  $\sim^{\text{X}}(\text{Na}_{0.5}\text{Ca}_{0.2}\square_{0.3})^{\text{Y}}(\text{Al}_{1.4}\text{Li}_{1.4}\text{Mn}_{0.1}^{2+}\square_{0.1})^{\text{Z}}\text{Al}_6^{\text{T}}(\text{Si}_{5.8}\text{B}_{0.2})\text{O}_{18}(\text{BO}_3)_3(\text{OH})_3^{\text{V}} [a = 15.824(5)$ ,  $c = 7.095(3)$  Å], and a colorless Li-bearing olenite from Koralpe, Styria, Austria (OLE), with the optimized formula  $\sim^{\text{X}}(\text{Na}_{0.4}\text{Ca}_{0.3}\square_{0.3})^{\text{Y}}(\text{Al}_{2.4}\text{Li}_{0.4}\square_{0.2})^{\text{Z}}\text{Al}_6^{\text{T}}(\text{Si}_{4.9}\text{B}_{1.0}\text{Al}_{0.1})\text{O}_{18}(\text{BO}_3)_3^{\text{V}}(\text{OH})_3^{\text{W}}[\text{O}_{0.6}(\text{OH}_{0.3}\text{F}_{0.1})]$  (Hughes et al. 2000), is shown in Table 5. The chemical data from LC1X shows higher  $\text{Li}_2\text{O}$  and  $\text{CaO}$  contents (Table 5) than the structure crystal LC1 (Table 4). Both samples were taken from the colorless rim from the same crystal. However, this crystal shows a zonation in Ca and Li (Ca content increases concomitantly with Li content). It is not clear if material that was more Ca- and Li-rich than the small structure crystal was included in the powdered material ( $\sim 20$  mg powder for the ICP-MS analysis). The Li-rich tourmalines studied are strongly enriched in LREEs compared to HREEs and exhibit negative Eu anomalies (Fig. 7). The sum of the REEs is relatively high in the Li-rich tourmalines (LC1X: 152.4 ppm; AFGANT: 70.2 ppm; Table 5). This simply cannot be explained by the fact that Ca minerals are more favorable common hosts to REE than Na minerals, because the sample OLE with  $\sim 1.7$  wt%  $\text{CaO}$  (average value from this crystal; Ertl et al. 1997; Ertl and Brandstätter 1998; Hughes et al. 2000) has a  $\text{CaO}$  value that lies between those of samples LC1X (2.15 wt%; Table 5) and AFGANT (1.24 wt%; Table 5), but has a distinctly lower total sum for REEs (19 ppm; Table 5).

Among the REEs, the values for Ce (71 ppm), La (47.2 ppm), and Pr (6.3 ppm) are relatively high in the elbaite from Madagascar (sample LC1X). The Al-rich tourmaline (sample OLE) displays a similar trend but the enrichment of the LREEs compared to the HREEs is not as strong. Raith et al. (2004) concluded that tourmaline does not preferentially fractionate specific REEs or groups of REEs during crystallization. Our Li-rich tourmaline samples are further enriched in Th [LC1X (4.4 ppm) > AFGANT (3.3 ppm) > OLE (1.1 ppm); Table 5]. Higher Th contents conform to the enrichment in LREE that

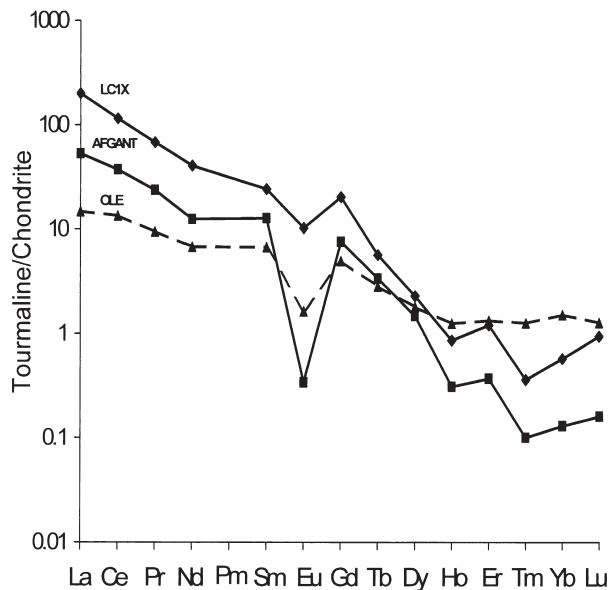


FIGURE 7. Chondrite-normalized REE pattern of three Al-Li-tourmalines. LCIX: elbaite from Anjanabonoina, Madagascar. AFGANT: elbaite from Nuristan, Afghanistan. OLE: olenite from Stoffhütte, Koralpe, Styria, Austria.

are geochemical analogs of Th. The sample with the highest Th content (LCIX; elbaite from Madagascar) shows the strongest enrichment of LREEs and a high  $La_N/Yb_N$  ratio of  $\sim 351$ . The elbaite samples (LCIX, AFGANT) from pegmatites, originating from highly fractionated granitic melts, are strongly enriched in LREEs compared to HREEs. In contrast, tourmalines (schorl-dravite series) from pegmatites from Nova Scotia, Canada (Konkatak et al. 2002), which are not related to conventional processes of late-stage fractionation of granitic magmas, show relatively low REE (3.0–4.2 ppm) and low  $La_N/Yb_N$  ratios of 1.2–1.8. In terms of trace-element composition, the elbaite from Madagascar crystallized in the most evolved pegmatite, the elbaite from Afghanistan crystallized in a highly evolved pegmatite, and the olenite from Koralpe, Austria, crystallized in a less-highly evolved pegmatite. We believe that these Li-bearing tourmalines mirror the REE distribution of the pegmatites in which they crystallized during the time of crystallization. These patterns seem to confirm an important role of the fractional crystallization process. A moderate-to-strong negative Eu anomaly in the REE patterns suggests feldspar fractionation to be an important process in the genesis of these pegmatites. The Sc content of the elbaite from Madagascar (139 ppm; Table 5) is one of the highest reported to date. Conklin and Slack (1983) described tourmaline from the Appalachian-Caledonian Orogen, with 170 ppm Sc. Lyakhovich and Lyakhovich (1983) reported 222 ppm Sc in a pegmatitic tourmaline. Pezzotta (2001b) described pegmatites (from Madagascar) of the Monazite-Thortveitite Subtype of the Rare Earth Type (NYF) that contain thortveitite ( $Sc, Y)_2[Si_2O_7]$  and beryls with up to several wt% Sc. Because of the relative high Sc and Ce content in tourmaline, the tourmaline-bearing pegmatites from Anjanabonoina may come close to the Monazite-Thortveitite Subtype.

## ACKNOWLEDGMENTS

We thank D. Decker, Oberboihingen, Germany, for providing the tourmaline samples and A. Wagner, Vienna, Austria, for preparing them. Special thanks to B.M. Laurs and A. Leuenberger for references and for helpful informations about liddicoatite samples from Madagascar, and to T. Meisel for references about the chondrite values. This paper is dedicated to Richard T. Liddicoat. This work was supported by NSF grants EAR-0003201 and EAR-9804768 to J.M.H. We sincerely thank E.S. Grew, F.C. Hawthorne, F.F. Foit, G.R. Rossman, and R. Thompson for their careful reviews of the manuscript.

## REFERENCES CITED

- Acosta-Vigil, A., London, D., Dewers, T.A., and Morgan, G.B., VI (2002) Dissolution of corundum and andalusite in  $H_2O$ -saturated haplogranitic melts at 800 °C and 200 MPa: Constraints on diffusivities and the generation of peraluminous melts. *Journal of Petrology*, 43, 1885–1908.
- Acosta-Vigil, A., London, D., Morgan, G.B., VI, and Dewers, T.A. (2003) Solubility of excess alumina in hydrous granitic melts in equilibrium with peraluminous minerals at 700–800 °C and 200 MPa, and applications of the aluminum saturation index. *Contributions to Mineralogy and Petrology*, 146, 100–119.
- Akizuki, M., Kuribayashi, T., and Kitakaze, A. (2001) Triclinic liddicoatite and elbaite in growth sectors of tourmaline from Madagascar. *American Mineralogist*, 86, 364–369.
- Arredondo, E.H., Rossman, G.R., and Lumpkin, G.R. (2001) Hydrogen in spessartine-almandine garnets as a tracer of granitic pegmatite evolution. *American Mineralogist*, 86, 485–490.
- Bloodaxe, E.S., Hughes, J.M., Dyar, M.D., Grew, E.S., and Guidotti, C.V. (1999) Linking structure and chemistry in the schorl-dravite series. *American Mineralogist*, 84, 922–928.
- Bosi, F. and Lucchesi, S. (2004) Crystal chemistry of the schorl-dravite series. *European Journal of Mineralogy*, 16, 335–344.
- Bruker AXS Inc. (2001) SAINTPLUS. Bruker AXS Inc., Madison, Wisconsin.
- Černý, P. (1991) Rare-element granitic pegmatites. Part I: Anatomy and internal evolution of pegmatite deposits. *Geoscience Canada*, 18, 49–67.
- Conklin, N.M. and Slack, J.F. (1983) Trace-element analyses of tourmaline from the Appalachian-Caledonian massive sulfide deposits. US Geological Survey Open-file Report, 83-890, 5 p.
- De Vito, C. (2002) Il Giacimento Gemmifero e ad Elementi Rari dell' Anjanabonoina, Betafo, Madagascar Centrale. Ph.D. thesis, University La Sapienza, Rome.
- Dirlam, D.M., Laurs, B.M., Pezzotta, F., and Simmons, W.B. (2002) Liddicoatite tourmaline from Anjanabonoina, Madagascar. *Gems and Gemology*, 38, 28–53.
- Dunn, P.J., Appleman, D.E., and Nelen, J.E. (1977) Liddicoatite, a new calcium end-member of the tourmaline group. *American Mineralogist*, 62, 1121–1124.
- Dyar, M.D., Taylor, M.E., Lutz, T.M., Francis, C.A., Guidotti, C.V., and Wise, M. (1998) Inclusive chemical characterization of tourmaline: Mössbauer study of Fe valence and site occupancy. *American Mineralogist*, 83, 848–864.
- Dyar, M.D., Wiedenbeck, M., Robertson, D., Cross, L.R., Delaney, J.S., Ferguson, K., Francis, C.A., Grew, E.S., Guidotti, C.V., Hervig, R.L., Hughes, J.M., Husler, J., Leeman, W., McGuire, A.V., Rhede, D., Rothe, H., Paul, R.L., Richards, L., and Yates, M. (2001) Reference Minerals for the Microanalysis of Light Elements. *Geostandards Newsletter*, 25, 441–463.
- Ertl, A. and Brandstätter, F. (1998) Olenit mit Borüberschuß aus einem Metapegmatit östlich der Stoffhütte, Koralpe, Steiermark. *Österreichische Akademie der Wissenschaften, Mathematisch-Naturwissenschaftliche Klasse, Abt. I, Mitteilungen der Abteilung für Mineralogie am Landesmuseum Joanneum*, 62/63, 3–21.
- Ertl, A. and Hughes, J.M. (2002) The crystal structure of an aluminum-rich schorl overgrown by boron-rich olenite from Koralpe, Styria, Austria. *Mineralogy and Petrology*, 75, 69–78.
- Ertl, A., Pertlik, F., and Bernhardt, H.-J. (1997) Investigations on olenite with excess boron from the Koralpe, Styria, Austria. *Österreichische Akademie der Wissenschaften, Mathematisch-Naturwissenschaftliche Klasse, Abt. I, Anzeiger*, 134, 3–10.
- Ertl, A., Hughes, J.M., and Marler, B. (2001) Empirical formulae for the calculation of  $\langle T-O \rangle$  and  $\langle X-O \rangle$  bond lengths in tourmaline and relations to tetrahedrally-coordinated boron. *Neues Jahrbuch Mineralogie Monatshefte*, 12, 548–557.
- Ertl, A., Hughes, J.M., Prowatke, S., Rossman, G.R., London, D., and Fritz, E.A. (2003) Mn-rich tourmaline from Austria: structure, chemistry, optical spectra, and relations to synthetic solid solutions. *American Mineralogist*, 88, 1369–1376.
- Ertl, A., Pertlik, F., Dyar, M.D., Prowatke, S., Hughes, J.M., Ludwig, T., and Bernhardt, H.-J. (2004a) Olenite with tetrahedrally coordinated  $Fe^{3+}$  from Eibenstein, Austria: structural, chemical, and Mössbauer data. *Canadian Mineralogist*, 42, 1057–1063.
- Ertl, A., Schuster, R., Prowatke, S., Brandstätter, F., Ludwig, T., Bernhardt, H.-J., Koller, F., and Hughes, J.M. (2004b) Mn-rich tourmaline and fluorapatite in a Variscan pegmatite from Eibenstein an der Thaya, Bohemian massif, Lower Austria. *European Journal of Mineralogy*, 16, 551–560.
- Ertl, A., Rossman, G.R., Hughes, J.M., Prowatke, S., and Ludwig, T. (2005)

- Mn-bearing "oxy-rossmanite" with tetrahedrally-coordinated Al and B from Austria: structure, chemistry, and infrared and optical spectroscopic study. *American Mineralogist*, 90, 481–487.
- Fernandez, A., Huber, S., Schreurs, G., Villa, I., and Rakotondrazafy, M. (2001) Tectonic evolution of the Ireimo region (central Madagascar) and implications for Gondwana assembly. *Gondwana Research*, 4/2, 156–168.
- Frost, R.L., Ding, Z., and Klopogge, J.T. (2000) The application of near-infrared spectroscopy to the study of brucite and hydroxalite structure. *Canadian Journal of Analytical Sciences and Spectroscopy*, 45, 96–102.
- Frost, R.L., Kristy, L.E., Moses, O.A., and Matt, L.W. (2005) Near-infrared spectroscopy of autunites. *Spectrochimica Acta, Part A, Molecular and Biomolecular Spectroscopy*, 61, 367–372.
- Grice, J.D. and Ercit, T.S. (1993) Ordering of Fe and Mg in the tourmaline crystal structure: the correct formula. *Neues Jahrbuch Mineralogie Abhandlungen*, 165, 245–266.
- Hawthorne, F.C. (2002) Bond-valence constraints on the chemical composition of tourmaline. *Canadian Mineralogist*, 40, 789–797.
- Henry, D.J. (2005) Fluorine—X-site vacancy avoidance in natural tourmaline: internal vs. external control. 2005 Goldschmidt Conference, May 20–25, Moscow, Idaho, Abstracts Volume, abstract no. 1318.
- Henry, D.J. and Dutrow, B. (1996) Metamorphic tourmaline and its petrologic applications. In E.S. Grew and L.M. Anovitz, Eds., *Boron: Mineralogy, Petrology, and Geochemistry*, 33, p. 503–557. *Reviews in Mineralogy and Geochemistry*, Mineralogical Society of America, Chantilly, Virginia.
- Hughes, J.M., Ertl, A., Dyar, M.D., Grew, E., Shearer, C.K., Yates, M.G., and Guidotti, C.V. (2000) Tetrahedrally coordinated boron in a tourmaline: Boron-rich olenite from Stoffhütte, Koralpe, Austria. *Canadian Mineralogist*, 38, 861–868.
- Hughes, J.M., Ertl, A., Dyar, M.D., Grew, E., Wiedenbeck, M., and Brandstätter, F. (2004) Structural and chemical response to varying  $^{11}\text{B}$  content in zoned Fe-bearing olenite from Koralpe, Austria. *American Mineralogist*, 89, 447–454.
- Hughes, K.-A., Hughes, J.M., and Dyar, M.D. (2001) Chemical and structural evidence for  $^{11}\text{B} \leftrightarrow ^{10}\text{B}$  substitution in natural tourmalines. *European Journal of Mineralogy*, 13, 743–747.
- Johnson, E.A. and Rossman, G.R. (2003) The concentration and speciation of hydrogen in feldspars using FTIR and  $^1\text{H}$  MAS NMR spectroscopy. *American Mineralogist*, 88, 901–911.
- Kalt, A., Schreyer, W., Ludwig, T., Prowatke, S., Bernhardt, H.-J., and Ertl, A. (2001) Complete solid solution between magnesian schorl and lithian excess-boron olenite in a pegmatite from Koralpe (eastern Alps, Austria). *European Journal of Mineralogy*, 13, 1191–1205.
- Kontak, D.J., Dostal, J., Kyser, T.K., and Archibald, D.A. (2002) A petrological, geochemical, isotopic and fluid inclusion study of 370 Ma pegmatite-aplite sheets, Peggys Cove, Nova Scotia, Canada. *Canadian Mineralogist*, 40, 1249–1286.
- Kovács, L., Lengyel, K., Péter, Á., Polgár, K., and Beran, A. (2003) IR absorption spectroscopy of water in  $\text{CsLiB}_3\text{O}_{10}$  crystals. *Optical Materials*, 24, 457–463.
- Lyakhovich, T.T. and Lyakhovich, V.V. (1983) New data on accessory-mineral compositions. *Geochemistry International*, 20, 91–108.
- MacDonald, D.J. and Hawthorne, F.C. (1995) The crystal chemistry of  $\text{Si} \leftrightarrow \text{Al}$  substitution in tourmaline. *Canadian Mineralogist*, 33, 849–858.
- Marler, B. and Ertl, A. (2002) Nuclear magnetic resonance and infrared spectroscopic study of excess-boron olenite from Koralpe, Styria, Austria. *American Mineralogist*, 87, 364–367.
- Marschall, H.R. and Ludwig, T. (2004) The low-boron contest: minimising surface contamination and analysing boron concentrations at the ng/g-level by secondary ion mass spectrometry. *Mineralogy and Petrology*, 81, 265–278.
- Marschall, H.R., Ertl, A., Hughes, J.M., and McCammon, C. (2004) Metamorphic Na- and OH-rich disordered dravite with tetrahedral boron, associated with omphacite, from Syros, Greece: chemistry and structure. *European Journal of Mineralogy*, 16, 817–823.
- McDonough, W.F. and Sun, S.-S. (1995) Composition of the Earth. *Chemical Geology*, 120, 223–253.
- Ottolini, L., Bottazzi, P., and Vannucci, R. (1993) Quantification of lithium, beryllium, and boron in silicates by secondary Ion Mass Spectrometry using conventional energy filtering. *Analytical Chemistry*, 65, 1960–1968.
- Palme, H. (1988). Chemical abundances in meteorites. In G. Klare, Ed., *Reviews in Modern Astronomy*, p. 28–51. Springer, Berlin.
- Pankrath, R. and Langer, K. (2002) Molecular water in beryl,  $[\text{LiAl}_2[\text{Be}_3\text{Si}_6\text{O}_{18}]]_n\text{H}_2\text{O}$ , as a function of pressure and temperature: An experimental study. *American Mineralogist*, 87, 238–244.
- Pearce, N.J.G., Perkins, W.T., Westgate, J.A., Gorton, M.P., Jackson, S.E., Neal, C.R., and Chenery, S.P. (1997) A compilation of new and published major and trace element data for NIST SRM 610 and NIST SRM 612 glass reference materials. *Geostandards Newsletter*, 21, 115–144.
- Petters, S.W. (1991) *Regional Geology of Africa*, Lecture Notes in Earth Science Series, 722 p. Springer-Verlag, New York.
- Pezzotta, F. (2001a) Madagascar—A mineral and gemstone paradise. *extraLapis English*, 1, 97 p.
- — — (2001b) Short note on the classification of Malagasy pegmatites. In F. Pezzotta and Wm.B. Simmons, Eds., *Field course on the rare element pegmatites of Madagascar*. Technical program and field trip guidebook June 11–22, 2001, Antananarivo, Madagascar. 14–16. UNESCO-IUGS-IGCP.
- Pezzotta, F. and Franchi, M. (1997) Mirolitic shallow depth pegmatites of the Betafo and Antsirabe areas, central Madagascar; genetic inferences. In R. Cox and L.D. Ashwal, Eds., *Proceedings of the UNESCO-IUGS-IGCP-348/368 International Field Workshop on Proterozoic Geology of Madagascar*. Antananarivo, August, 16–30, *Gondwana Research Group Miscellaneous Publication No. 5*, 71 pp.
- Prasad, P.S.R., Prasad, K.S., and Thakur, N.K. (2006) FTIR signatures of type-II clathrates of carbon dioxide in natural quartz veins. *Current Science*, 90, 1544–1547.
- Raith, J.G., Riemer, N., and Meisel, T. (2004) Boron metasomatism and behaviour of rare earth elements during formation of tourmaline rocks in the eastern Arunta Inlier, central Australia. *Contribution Mineralogy Petrology*, 147, 91–109.
- Roedder, E., Ed. (1984) *Fluid inclusions*, vol. 12. *Reviews in Mineralogy*, Mineralogical Society of America, Chantilly, Virginia.
- Schreyer, W., Hughes, J.M., Bernhardt, H.-J., Kalt, A., Prowatke, S., and Ertl, A. (2002) Reexamination of olenite from the type locality: detection of boron in tetrahedral coordination. *European Journal of Mineralogy*, 14, 935–942.
- Selway, J.B., Novák, M., Hawthorne, F.C., Černý, P., Ottolini, L., and Kyser, T.K. (1998) Rossmanite,  $[\text{LiAl}_2] \text{Al}_6\text{Si}_6\text{O}_{18} (\text{BO}_3)_3 (\text{OH})_4$ , a new alkali-deficient tourmaline: description and crystal structure. *American Mineralogist*, 83, 896–900.
- Tagg, S.L., Cho, H., Dyar, M.D., and Grew, E.S. (1999) Tetrahedral boron in naturally occurring tourmaline. *American Mineralogist*, 84, 1451–1455.
- Wasson, J.T. and Kallemeyn, G.W. (1988) Composition of chondrites. *Philosophical Transactions of the Royal Society of London, Series A, Mathematical and Physical Sciences*, 352(1587), 535–544.
- Wood, D.L. and Nassau, K. (1967) Infrared spectra of foreign molecules in beryl. *Journal of Chemical Physics*, 47, 2220–2228.
- — — (1968) The characterization of beryl and emerald by visible and infrared spectroscopy. *American Mineralogist*, 55, 727–734.
- Wright, S.E., Foley, J.A., and Hughes, J.M. (2000) Optimization of site-occupancies in minerals using quadratic programming. *American Mineralogist*, 85, 524–531.

MANUSCRIPT RECEIVED FEBRUARY 23, 2006

MANUSCRIPT ACCEPTED MAY 5, 2006

MANUSCRIPT HANDLED BY EDWARD GREW